

We are IntechOpen, the world's leading publisher of Open Access books Built by scientists, for scientists

5,000

Open access books available

125,000

International authors and editors

140M

Downloads

Our authors are among the

154

Countries delivered to

TOP 1%

most cited scientists

12.2%

Contributors from top 500 universities



WEB OF SCIENCE™

Selection of our books indexed in the Book Citation Index
in Web of Science™ Core Collection (BKCI)

Interested in publishing with us?
Contact book.department@intechopen.com

Numbers displayed above are based on latest data collected.
For more information visit www.intechopen.com



Material Removal Mechanism and Force Model of Nanofluid Minimum Quantity Lubrication Grinding

Yanbin Zhang, Changhe Li, Yongjun Zhao, Xin Cui, Xiufang Bai, Mingzheng Liu, Yali Hou, Min Yang, Naiqing Zhang, Heju Ji, Xiaoming Wang and Teng Gao

Abstract

Numerous researchers have developed theoretical and experimental approaches to force prediction in surface grinding under dry conditions. Nevertheless, the combined effect of material removal and plastic stacking on grinding force model has not been investigated. In addition, predominant lubricating conditions, such as flood, minimum quantity lubrication (MQL), and nanofluid minimum quantity lubrication (NMQL), have not been considered in existing force models. In this study, material removal mechanism under different lubricating conditions was researched. An improved theoretical force model that considers material removal and plastic stacking mechanisms was presented. Grain states, including cutting and ploughing, are determined by cutting efficiency (β). The influence of lubricating conditions was also considered in the proposed force model. Simulation was performed to obtain the cutting depth (a_g) of each “dynamic active grain.” Parameter β was introduced to represent the plastic stacking rate and determine the force algorithms of each grain. The aggregate force was derived through the synthesis of each single-grain force. Finally, pilot experiments were conducted to test the theoretical model. Findings show that the model’s predictions were consistent with the experimental results, with average errors of 4.19% and 4.31% for the normal and tangential force components, respectively.

Keywords: grinding, minimum quantity lubrication, nanofluid, material removal mechanism, force model

1. Introduction

With need of green manufacturing, nanofluid minimum quantity lubrication (NMQL) was introduced to grinding [1, 2], which could effectively improve cooling and lubricating performance compared to conventional dry or flood conditions [3, 4]. Furthermore, with the deeper understanding of grinding mechanism and the development of process technology for difficult-to-grinding material, advancement in the experiment has been rapidly made [5–7]. Of course, with such a demand from

designing of grinding technological parameter, material removal mechanism and force model under NMQL condition are of key importance.

Material removal mechanism, here, mostly refers to deformation, fracture process, and strain rate of material in grinding zone, as well as mechanical behavior of chips and furrow formation [8, 9], which relates to grinding parameters and cooling/lubricating conditions [10, 11]. For dry grinding, the experimental studies have been carried out, and force, temperature, shape of chips, and surface quality were observed, which showed special phenomenon when higher speed (i.e., speed effect) and lower cutting depth (i.e., size effect) were used. Nevertheless, material removal mechanism under NMQL condition is vacant and important, which should be researched deeply.

Force model of grinding, in general, was vector sum of sliding force, cutting force, and ploughing force of all dynamic active grains in grinding zone. Many researches were carried out to establish grinding force model under dry condition. Werner [12] derived a grinding force equation with two parts (cutting force and sliding force), which was adopted by Malkin and Hwang [13], Li et al. [14], Younis et al. [15], and Tang et al. [16]. To obtain grain stages and numbers, Rayleigh's probability density distribution [17, 18] and normal distribution [19] were used to describe cutting depth of grain [20]. Except for steel material, the grinding force model was also researched for single crystal sapphire [21], SiCp/Al composites [22], complex optical mirrors [23], etc. However, previous models were limited at three aspects:

- i. The average cutting depths were used for each grain states (i.e., cutting, ploughing, sliding), which cannot represent the actual situation in the grinding zone [24].
- ii. The critical depth of cutting and ploughing was determined by an experience-based evaluation method: "when the grain-cutting depth reached 0.05 times of the radius of cutting grains, cutting action occurred" [25–27]. It's imprecise for different material.
- iii. The number of "static active grains" was presented to develop force models, which are not considered interference effect of grains on each other [28–32].
- iv. The lubricating condition was not considered.

This chapter proposes an improved theoretical force model that takes the material removal and plastic stacking mechanism into consideration. The scratch tests reveal the relationship between cutting depth (a_g) and cutting efficiency (β) to distinguish the cutting and ploughing grains and determine the force algorithms of each grain. The tribological tests reveal the friction coefficients under different grinding lubricating conditions to calculate the frictional force of each grain. In addition, the a_g of each "dynamic active grain" in the grinding zone is obtained by simulation, to assist the development of the grinding force model. To verify the proposed model, grinding experiments were performed, and force values were obtained and compared with predictive values.

2. Material removal mechanism of NMQL grinding

2.1 Deformation and strain rate

The material deformation mechanism in the grinding zone with single abrasive particle is shown in **Figure 1**. The material deformation mechanism in the chip

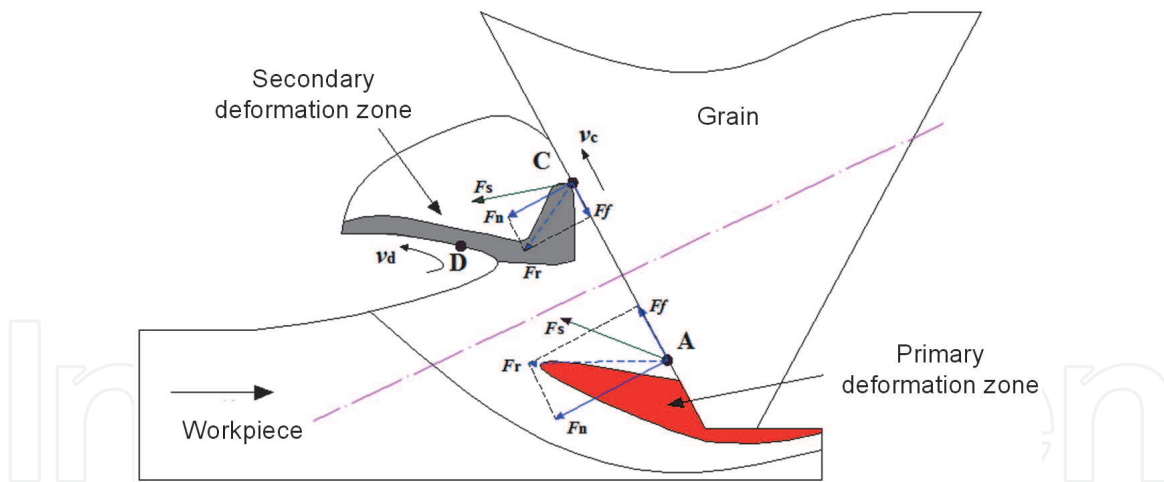


Figure 1.
 Deformation mechanism of material in the cutting zone.

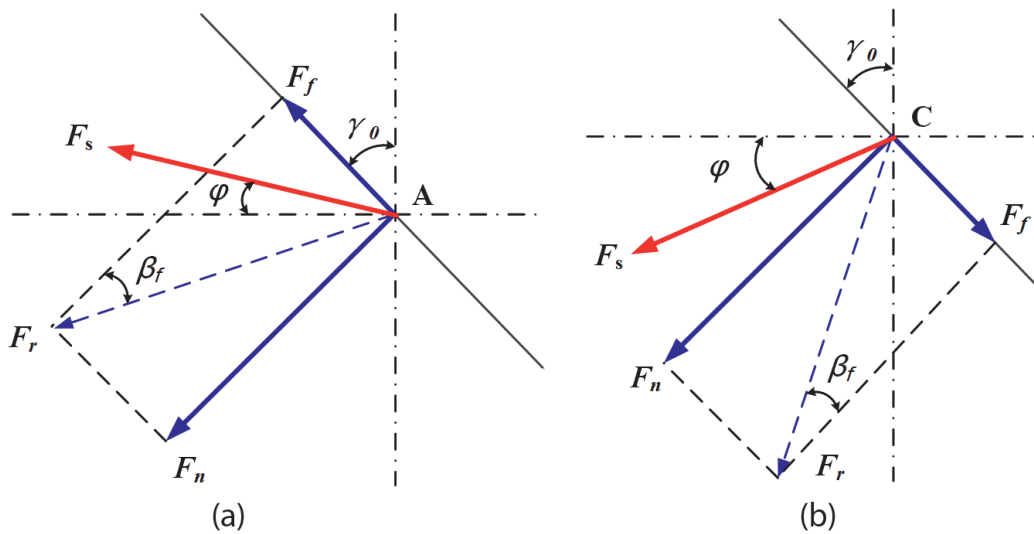


Figure 2.
 Stress analysis of the workpiece material in the cutting zone. (a) Primary deformation zone and (b) secondary deformation zone.

formation zone during the grinding machining is identical with that during cutting machining, and primary deformation zone and secondary deformation zone simultaneously exist.

Ding et al. [33] conducted an analog simulation of high-temperature cutting of nickel-based alloy workpiece material with single abrasive particle and also observed the abovementioned phenomenon. Different from cutting machining, the negative rake cutting form of abrasive particle leads to a different mechanical action mechanism between abrasive particle/grinding chips; the calculation formulas of shear angle φ , frictional angle β_f , and strain rate are also changed, but the impact trends of grinding process parameters and lubricating conditions on material removal mechanism are totally the same. The force analysis of the grinding zone of single abrasive particle is shown in **Figure 2**, and material force bearing and deformation mechanism can be described as follows:

- i. In the primary deformation zone, **Figure 2(a)** is force analysis graph of point A, and the resultant force of frictional force F_f and extrusion force F_n is F_r . According to the mechanical theory of material, the included angle between rupture chip formation direction (direction F_s of shear zone) and resultant force F_r is $\pi/4$, and shear angle φ is on horizontal line; at the time, frictional force F_f

exerts a promoting effect on rupture chip formation of the material upward along the abrasive particle/cutting chip interface. Hence, the expression of shear angle φ is solved according to geometrical relations of several angles as below:

$$\varphi_1 = \frac{\pi}{4} + \beta_f - \gamma_0 \quad (1)$$

The ratio of thickness to length of grinding chips formed through cutting machining of abrasive particle is about 1/100, so negative rake is $\gamma_0 \approx \theta/2$ and frictional angle is $\beta_f = \arctan(\mu)$ under abrasive particle cutting, where μ is frictional coefficient between rake face of abrasive particle/cutting chips. The relational expression between γ_0 and β is substituted into Eq. (1) to obtain:

$$\varphi_1 = \frac{\pi}{4} + \arctan \mu - \frac{\theta}{2} \quad (2)$$

- ii. In the secondary deformation zone, **Figure 2(b)** is force analysis chart, where the resultant force of frictional force F_f and extrusion force F_n is F_r . According to the mechanical theory of material, the included angle between rupture chip formation direction (direction F_s of shear zone) and resultant force F_r is $\pi/4$, and shear angle φ is below the horizontal line; at the time, frictional force F_f exerts an inhibitory effect on flow of grinding chips downward along the abrasive particle/cutting chip interface. After kinetic analysis, speed of movement on abrasive particle/grinding chip interface is low due to frictional force, but the speed on free face of grinding chips is high; under high-speed cutting condition, transient speed difference is generated between abrasive particle/grinding chip interface and free face of grinding chips due to high strain rate of grinding chips, thus generating a shear zone and forming the secondary deformation zone. Hence, the expression of shear angle φ can be solved according to geometrical relations of several angles as:

$$\phi_2 = \beta_f + \gamma_0 - \frac{\pi}{4} = \arctan \mu + \frac{\theta}{2} - \frac{\pi}{4} \quad (3)$$

For high-speed grinding machining, the change of strain rate is the primary factor influencing the material removal mechanism. The strain rate reaches as high as 10^4 – 10^5 s^{-1} in the cutting machining process, but for low-speed grinding machining ($V_s \leq 30 \text{ m/s}$), the strain rate of material removal reaches up to 10^7 – 10^8 s^{-1} because of negative rake characteristic of abrasive particle. Therefore, it's speculated that the strain rate under high-speed grinding machining condition is higher than that under low-speed grinding machining condition of grinding wheel by 1 or 2 orders of magnitudes. Under high-speed grinding machining condition, the strain hardening effect and strain strengthening effect caused by strain rate of material deformation generate a remarkable effect on the material removal mechanism. Jin and Stephenson [34] established the equation of shear strain in the shear zone of abrasive particle and strain rate. Taking maximum undeformed cutting thickness and shear angle in the primary deformation zone and secondary deformation zone into account, strain rate of grinding chips in the two deformation zones could be calculated by the following equations:

$$\dot{\gamma}_1 = \frac{\lambda v_s^2 \cos\left(\frac{\theta}{2}\right) \sin\left(\frac{\pi}{4} + \arctan \mu - \frac{\theta}{2}\right)}{\pi v_w \sqrt{a_p D} \cos\left(\frac{\pi}{4} + \arctan \mu\right)} \quad (4)$$

$$\gamma_2 = - \frac{\lambda v_s^2 \cos\left(\frac{\theta}{2}\right) \sin\left(\arctan \mu + \frac{\theta}{2} - \frac{\pi}{4}\right)}{\pi v_w \sqrt{a_p D} \cos\left(\arctan \mu + \theta - \frac{\pi}{4}\right)} \quad (5)$$

where φ is shear angle, θ is vertex angle of abrasive particle, λ_1 is average length-width ratio in the shear zone ($\lambda_1 = 6-12$), v is cutting speed of abrasive particle, and $v \approx V_s$ is for single abrasive particle grinding.

It can be known from Eq. (4) that factors influencing deformational strain rate of workpiece material during the cutting process with single abrasive particle include grinding parameters, abrasive particle shape, and lubrication characteristics of abrasive particle/grinding chip interface. In this study, as $V_s/V_w = 1 \times 10^4$ and abrasive particle shape are unchanged, the influence trends of grinding speed V_s , grinding depth V_w , and grinding coefficient μ on shear rate will be hereby discussed.

As shown in **Figure 3(a)**, when other parameters remain unchanged, the strain rates in both primary shear zone and secondary shear zone present a linear growth trend when V_s increases from 30 to 120. In comparison with the primary deformation zone, the strain rate in the secondary deformation zone has a higher growth rate.

According to **Figure 3(b)**, when the frictional coefficient μ gradually increases, the strain rate in the primary deformation zone presents an increasing trend of quadratic function, because the frictional force in the primary deformation zone exerts a gaining effect on material removal and the strain rate increases with frictional force, which is better for chip formation. In the secondary deformation zone, as the frictional coefficient μ increases from small to great (characterizing lubricating condition), the strain

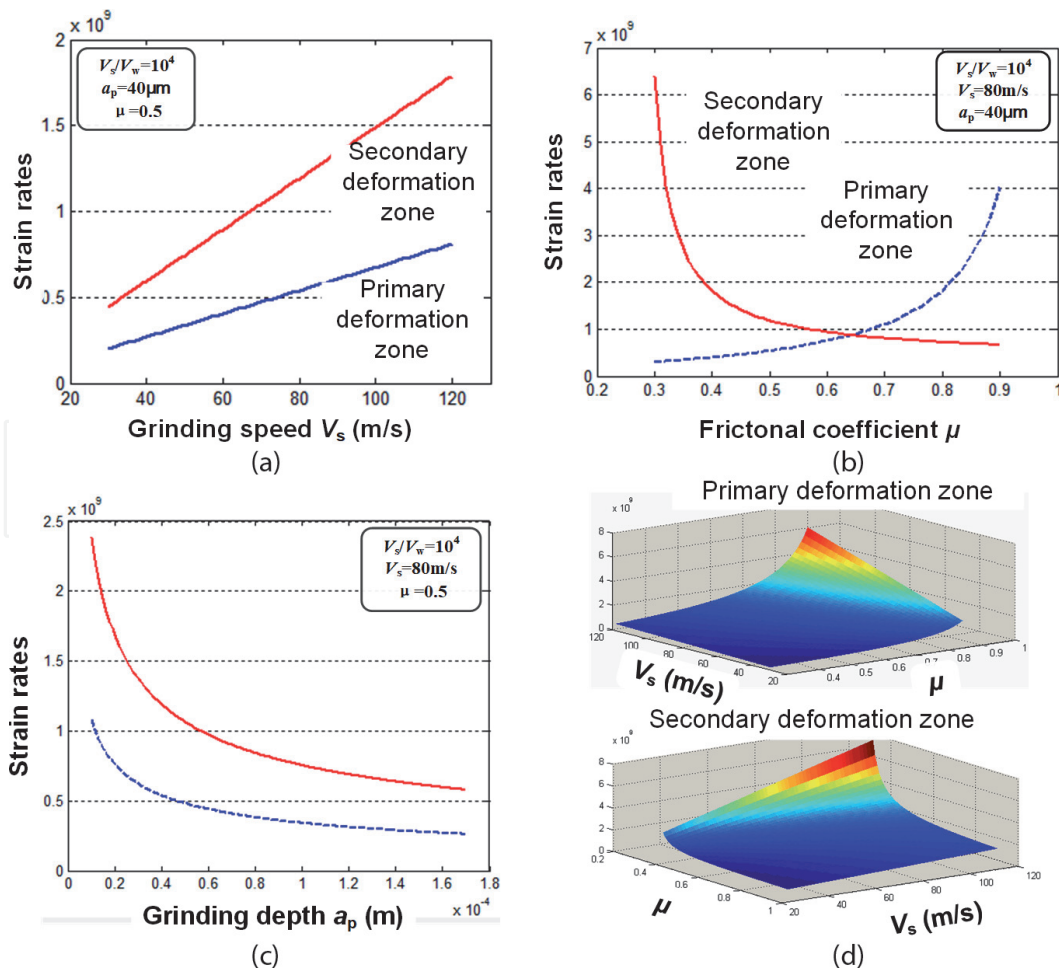


Figure 3. Strain rate under different grinding parameters and frictional coefficient. (a) Influence of grinding speed, (b) influence of frictional coefficient, (c) influence of grinding depth and (d) two-factor analysis.

rate in the secondary deformation zone presents a declining trend of quadratic function, the frictional force in the primary deformation zone prevents grinding chips from flowing out, and flow direction of grinding chips is gradually turned from towards abrasive particle into along the surface of abrasive particle, so the strain rate gradually declines. As shown in **Figure 3(c)**, the strain rate presents a linear declining trend due to increase of grinding depth. As this study focuses on speed effect and lubricating effect in the high-speed grinding machining, in consideration of impact trends of grinding speed and frictional coefficient on strain rate, **Figure 3(d)** shows the variation trend graphs of the primary deformation zone and secondary deformation zone under the influence of grinding speed and frictional coefficient.

2.2 Mechanism of chip formation

2.2.1 Theoretical research

Impact dynamics describes material deformation behaviors under high speed as an adiabatic shear process. Adiabatic shear effect refers to constitutive instability (thermal viscoplastic instability) of the material under impact load. Extremely strain rate exists in the material removal shear zone under the action of impact load, and the shear zone is a thermal insulating environment within a very short time. At the time, nonelastic energy in the material deformation process is converted into a large quantity of grinding heat, which leads to abrupt temperature rise of the material in the shear zone and declination of material hardness (softening) under temperature rise. The softening effect exceeds strain hardening effect and strain strengthening effect, and thus shear zone is formed and material instability is caused. Hence, the chip formation process under the effect of abrasive particle is dynamic stress and thermal force coupling action process under a high strain rate.

The removal process of metal material derives from plastic deformation after the material strain increases. In the previous studies, scholars have conducted a large quantity of dynamic material tensile tests [35], proving strain hardening and strain strengthening phenomena. As shown in **Figure 4**, the material removal process with the change of strain rate can be divided into the three following types according to the stress-strain curve:

As shown in **Figure 5(a)**, under quasi-static conditions, the material deformation stress will increase obviously with the strain, indicating that notable strain hardening effect happens to the workpiece material. Grinding chips will be formed after the stress increases to material breaking limit σ_{b1} , and free face of cutting chips presents periodic upheaval (bamboo shape), which is caused by extruding deformation in the grinding chip formation process; however, the strain rate of material deformation is low because of low speed, and no obvious shear zone is formed.

As shown in **Figure 5(b)**, under high strain rate, assume that the shear zone of grinding chips is in an isothermal environment: the material deformation stress in the strain hardening phase is far higher than that under quasi-static conditions, and this phenomenon is called “strain strengthening effect” of plastic deformation of material, and its deformational resistance is enhanced under strain strengthening effect. At the time, as abrasive particle has a strong impact effect on the material, workpiece material forms shear layers under high strain rate so as to form grinding chips, and rupture stress limit between shear layers is breaking limit σ_{b2} of the material under high strain rate. Free face of grinding chips presents notable periodic shear slippage layer, and the slippage distance of shear layer under high strain condition is obviously higher than that under quasi-static state; and the higher the speed, the higher the strain rate, and the greater the slippage distance of shear layer; and even radical rupture and separation between shear layers is caused by bluff-type rupture process.

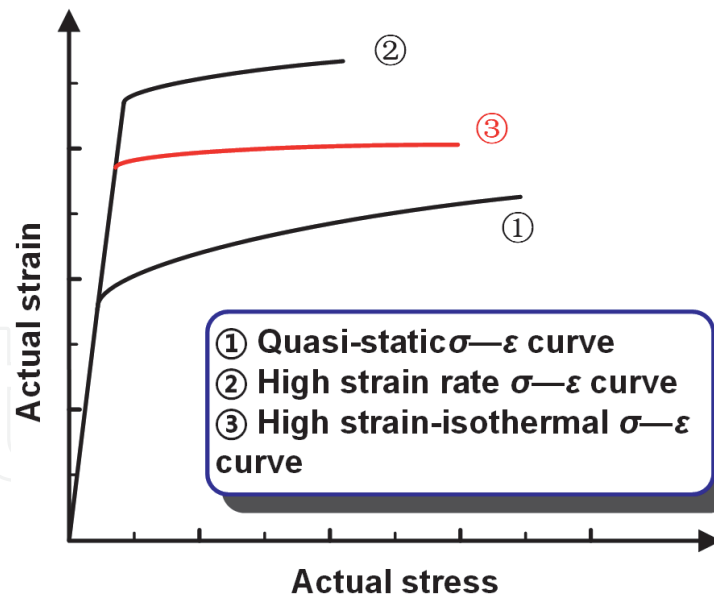


Figure 4.
 Stress-strain curve under “velocity effect.”

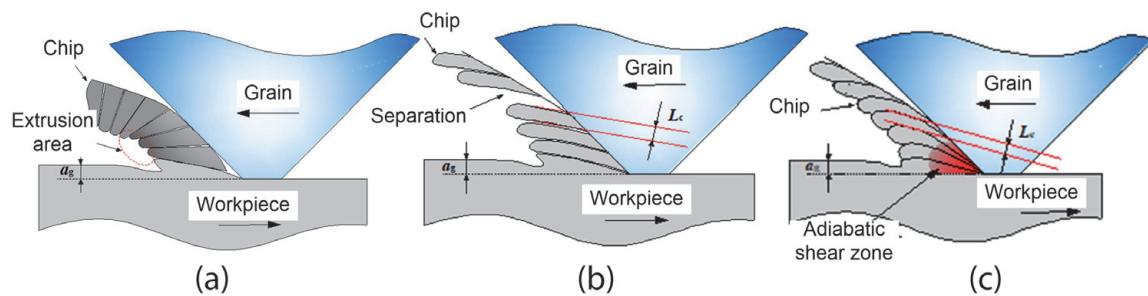


Figure 5.
 Chip-forming mechanism under (a) quasi-static, (b) high strain isothermal, and (c) high strain condition.

As shown in **Figure 5(c)**, in consideration of temperature rise at abrasive particle/grinding chip interface under high strain rate, the plastic deformation process of the material at the time is a comprehensive result of strain hardening effect and thermal softening effect, namely, adiabatic shear process. In **Figure 4**, the stress-strain curve is between quasi-static curve (curve 1) and high strain isothermal condition (curve 2) under the action of adiabatic shear, because a large quantity of grinding heat softens the material so as to reduce deformational resistance under the action of strengthening strain rate. As the strain rate increases, the heat transferred to shear zone is also increasing, thermal softening effect becomes more obvious, and the breaking limit relation of the material under three boundary conditions is $\sigma_{b2} > \sigma_{b3} > \sigma_{b1}$. Material rupture and plastic flow after thermal softening simultaneously exist between shear layers of grinding chips.

Hence, the critical research hotspots regarding material removal mechanism under high-speed grinding conditions are to explore into influences of grinding parameters and lubricating conditions on strain strengthening effect and thermal softening effect and build an evaluation model.

2.2.2 Experimental research

SEM of chips were shown in **Figure 6**.

The grinding chip shapes are similar at the grinding speed of 40 m/s under three different working conditions, namely, continuous banding chips, because the material strain rate is low and thermal softening effect in the grinding zone is small under low grinding speed. When the grinding speed is 80 m/s, obvious shear zones

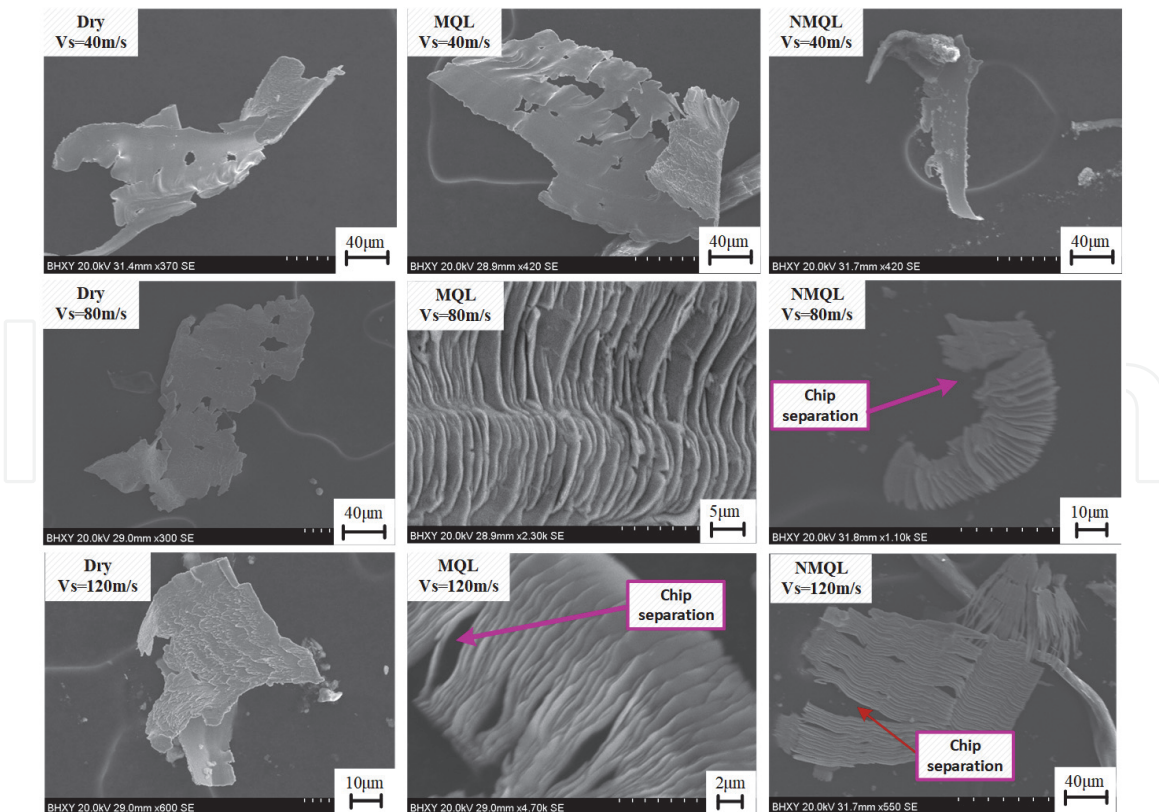


Figure 6.
Chip morphology at different lubricating conditions.

are observed on the free faces of the three types of grinding chips, indicating that under high grinding speed, the material experiences adiabatic shear during the forming process. Differently, the shear slippage layer spacing obtained under dry grinding conditions is small, that under MQL condition is larger, and that under NMQL is the largest, where even rupture takes place.

On the one hand, as the lubricating effect is enhanced and frictional coefficient is reduced in succession under the three lubricating conditions, the strain rate in the primary deformation zone at the same speed increases successively, so does shear slippage distance under the three conditions. On the other hand, the output of frictional heat is reduced as the lubricating effect is enhanced successively under the three conditions, and the heat quantity transferred out of the shear zone is increased as the cooling effect is enhanced successively under the three conditions. Therefore, the thermal softening effect during NMQL cutting chip formation process is lower than that under dry grinding condition. The shear layer slippage of grinding chips is mainly material rupture, followed by plastic flow, so shear layer spacing is larger, and grinding chips even rupture. Under the grinding speed of 120 m/s, the abovementioned rule is magnified again. Banding chips are still formed due to thermal softening effect under dry grinding, rupture of grinding chips induced by excessive shear layer spacing also appears under MQL condition, and the rupture under NMQL condition is further aggravated.

2.3 Mechanism of furrow formation and cutting efficiency

2.3.1 Plastic stacking effect

Cutting depth a_g (varies from 0 to a_{gmax}) and critical value a_{gc} were the key points for distinguishing ploughing and cutting stage. The value a_{gc} could be gotten from cutting experiment of single grain for different materials. The change rule could be concluded from **Figure 7**.

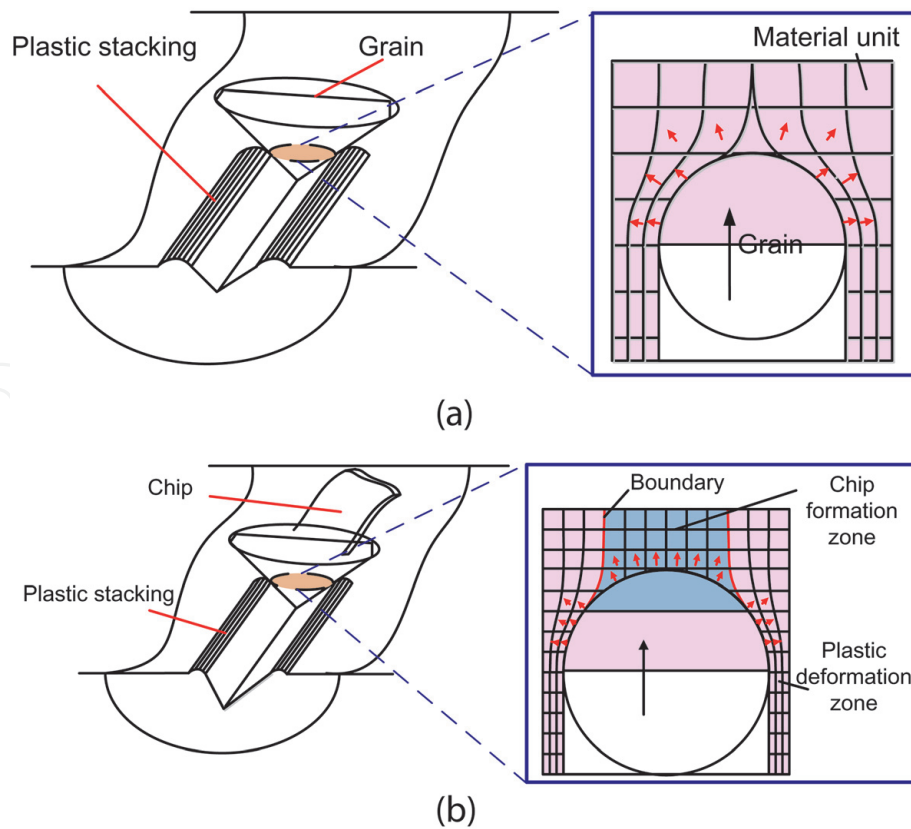


Figure 7. Material deformation behavior in cutting of a single grain. (a) Ploughing grain and (b) cutting grain.

- i. When $a_g \leq a_{gc}$ (ploughing stage). Material of workpiece flows upheaved and stacked at two sides of the furrows because the stress between material units is lower than fracture stress.
- ii. When $a_g > a_{gc}$ (cutting stage). Plastic stacking theory [36], which describes the coexistence phenomenon of material removal and elastic-plastic flow in grinding, is a good method to understand deformation behavior of material. Pink-colored material units in **Figure 7(b)** were the elastic-plastic flow part, and blue-colored units were the material removal part. However, a boundary was born between two regions.

Therefore, chip formation region ($0-\alpha_1$) and elastic-plastic flow region ($\alpha_1-\pi/2$) were defined in this paper, in which two were differentiated by critical value of angle α_1 , as shown in **Figure 8**. α_1 (could be calculated by cutting efficiency β [37]) was different when material changes:

$$\alpha_1 = \arccos(\sqrt{\beta}) \quad (6)$$

2.3.2 Model of $\beta(\alpha_g)$

Parameter β will increase from 0 to almost 1 when a_g increases [38]. Therefore the model of $\beta(\alpha_g)$ is the key point of grinding force prediction. Cutting experiment of single grain was carried out for stainless steel material (440 C, $R_a = 0.04-0.05 \mu\text{m}$). Surface topography of furrow is shown in **Figure 9**, and numerical fitting of $\beta(\alpha_g)$ was shown in **Figure 10**.

The $\beta(\alpha_g)$ curve present S-shaped (when a_g varies from 0 to $4.5 \mu\text{m}$) and further linear trend (when $a_g \geq 4.5 \mu\text{m}$). Therefore, Gompertz growth equation and Gaussian fitting were considered simultaneously, and piecewise function ($R^2 = 0.9945$) is shown as Eq. (7).

$$\beta(a_g) = \begin{cases} a_1 \cdot e^{-\left(\frac{a_g - b_1}{c_1}\right)^2} + a_2 \cdot e^{-\left(\frac{a_g - b_2}{c_2}\right)^2} + \dots + a_6 \cdot e^{-\left(\frac{a_g - b_6}{c_6}\right)^2}, & 0 \leq x \leq 3.8 \mu\text{m} \\ k \cdot e^{-a \cdot e^{-b \cdot a_g}}, & x > 3.8 \mu\text{m} \end{cases} \quad (7)$$

It could be observed from **Figure 10** that (i) three stages could be learned from curve slope of $\beta(\alpha_g)$; (ii) compared to study of Hahn [39], sliding stage (0–0.023 μm) is declined; and (iii) the transition stage exists between ploughing and cutting stage, which is different from traditional theory.

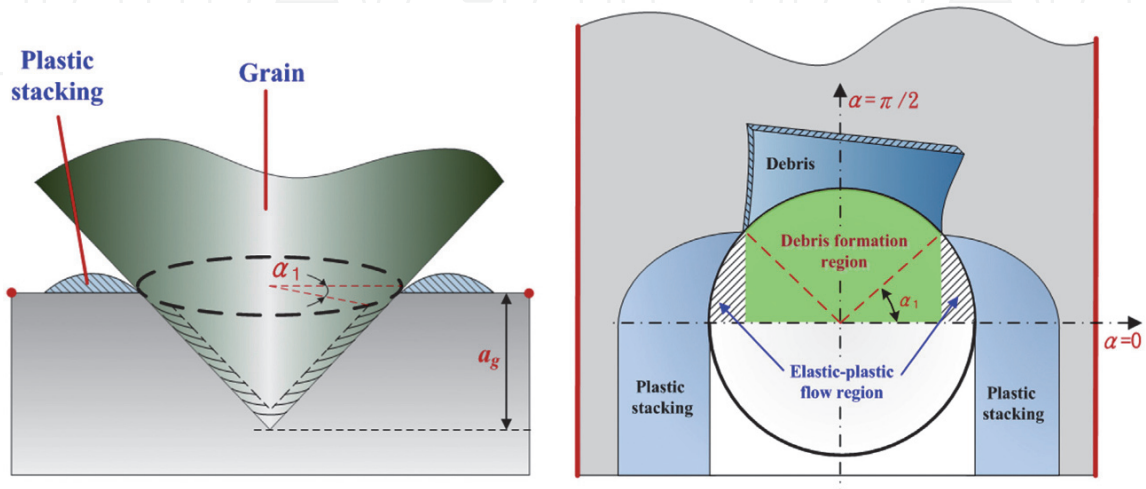


Figure 8.
Plastic stacking mechanism.

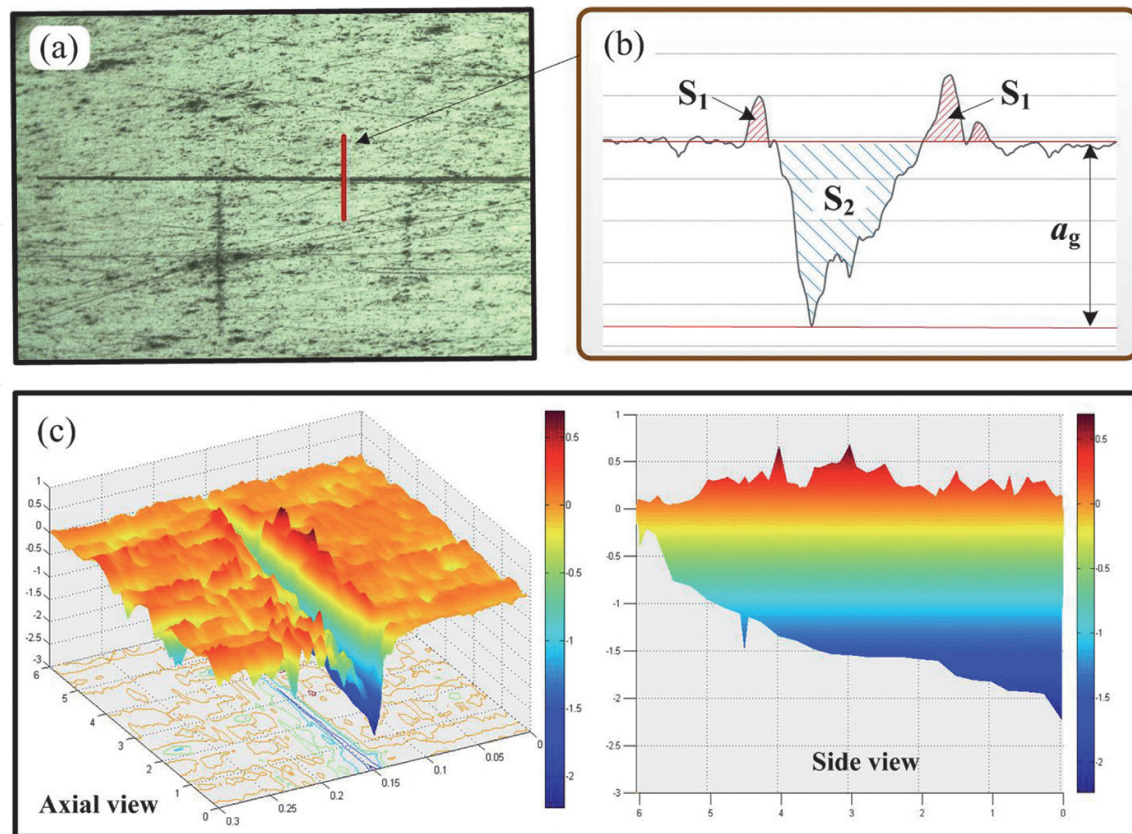


Figure 9.
Result of scratch tests. (a) Surface topography of furrow, (b) 2D profile curve of furrow, (c) 3D graph of furrow.

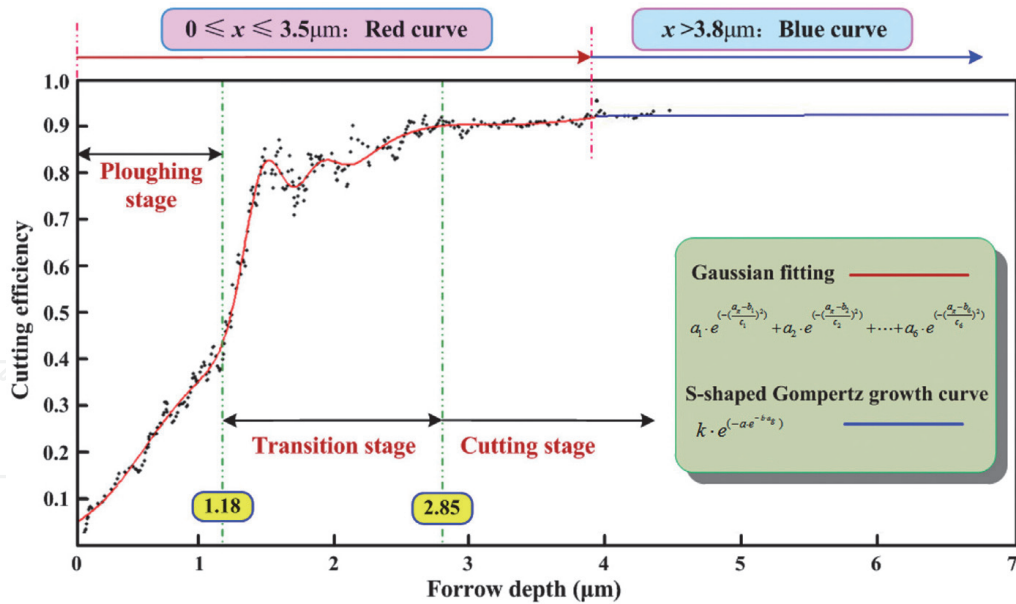


Figure 10.
 Equation of cutting efficiency (β).

3. Force model of single grain

3.1 Stress state of grain

As a premise for force model, analysis of stress state was carried out in this section according to the above results, as shown in **Figure 11**. Plastic flow is the material behavior, and equal stress value (yields stress δ_s) distributes on grain surface. The stresses at chip formation region (δ_0) and elastic-plastic flow region (δ_1) show characteristics as follows: (i) equal stress value (fracture stress δ_b) distributes on chip formation region and (ii) linear formula of stress distributes on elastic-plastic flow region, which varies from 0 to δ_b .

3.2 Force model in chip formation region ($\alpha_1 - \pi/2$)

δ_0 was composed of δ_{01} and δ_{02} in chip formation region. As shown in **Figure 12**, the integral unit (ds) can be expressed as:

$$d_s = \frac{a_g^2 \cdot \tan \theta}{2 \cdot \cos \theta} \cdot d\alpha \quad (8)$$

The plastic flow force equation $F_{tc(01)}(a_g)/F_{nc(01)}(a_g)$ in chip formation region could be calculated as:

$$F_{tc(01)}(a_g) = \int_{\alpha_1}^{\pi} \delta_s \cdot a_g^2 \cdot \tan \theta \cdot \cos \alpha \cdot d\alpha \quad (9)$$

$$F_{nc(01)}(a_g) = \int_{\alpha_1}^{\pi} \delta_s \cdot a_g^2 \cdot \tan^2 \theta \cdot d\alpha = \left(\frac{\pi}{2} - \alpha_1\right) \cdot \delta_s \cdot a_g^2 \cdot \tan^2 \theta \quad (10)$$

where θ is grain vertex angle and α_1 could be obtained by Eqs. (6) and (7), respectively.

The chip formation force equation $F_{tc(02)}(a_g)$ in chip formation region could be calculated as:

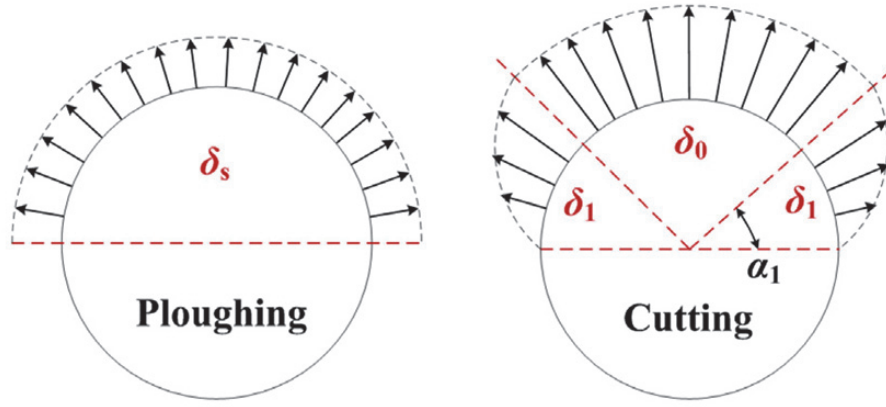


Figure 11. Schematic diagram of the grain stress state.

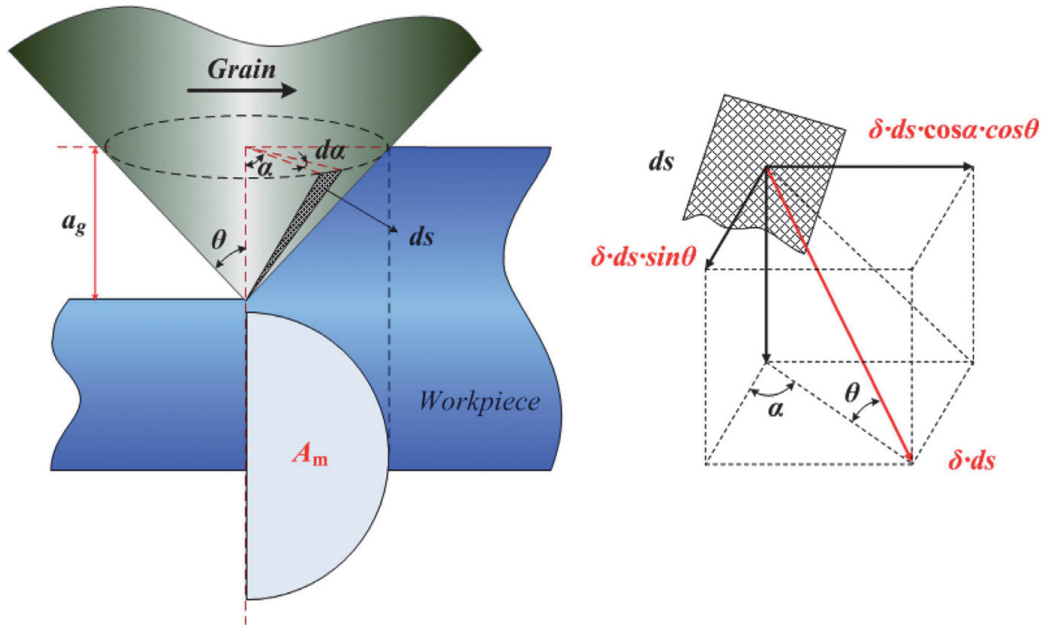


Figure 12. Calculation principle of cutting force.

$$F_{tc(02)}(a_g) = \int_{\alpha_1}^{\frac{\pi}{2}} \delta_{02} \cdot a_g^2 \cdot \tan \theta \cdot \cos \alpha \cdot d\alpha = \delta_b \cdot A_m \quad (11)$$

where A_m is area of the chip formation region and δ_{02} could be obtained by Eq. (11):

$$\delta_{02} = \frac{\pi \cdot \tan \theta}{2 \cdot (1 - \sin \alpha_1)} \cdot \delta_b \quad (12)$$

The normal force could be further calculated by Eqs. (11) and (12):

$$F_{nc(02)}(a_g) = \int_{\alpha_1}^{\frac{\pi}{2}} \delta_{02} \cdot a_g^2 \cdot \tan^2 \theta \cdot d\alpha = \frac{\pi \cdot (\frac{\pi}{2} - \alpha_1)}{2 \cdot (1 - \sin \alpha_1)} \cdot \delta_b \cdot a_g^2 \cdot \tan^3 \theta \quad (13)$$

In summary, δ_0 can be expressed as:

$$\delta_0 = \delta_{01} + \delta_{02} = \delta_s + \frac{\pi \cdot \tan \theta}{2 \cdot (1 - \sin \alpha_1)} \cdot \delta_b \quad (14)$$

3.3 Force model in elastic-plastic flow region (0– α_1)

The equation of δ_1 and force in elastic-plastic flow region show increased trend and could be calculated as:

$$\delta_1(\alpha) = \left[\frac{\delta_s}{\alpha_1} + \frac{\pi \cdot \delta_b \cdot \tan \theta}{\alpha_1 \cdot (1 - \sin \alpha_1)} \right] \cdot \alpha \quad (15)$$

$$F_{ic(1)}(a_g) = \int_0^{\alpha_1} \delta_1(\alpha) \cdot a_g^2 \cdot \tan \theta \cdot \cos \alpha \cdot d\alpha \quad (16)$$

$$F_{nc(1)}(a_g) = \int_0^{\alpha_1} \delta_1(\alpha) \cdot a_g^2 \cdot \tan^2 \theta \cdot d\alpha \quad (17)$$

Force equation of cutting grain could be obtained by the above equation:

$$F_{ic}(a_g) = F_{ic(1)}(a_g) + F_{ic(01)}(a_g) + F_{ic(02)}(a_g) \quad (18)$$

$$= \int_0^{\alpha_1} \delta_1(\alpha) \cdot a_g^2 \cdot \tan \theta \cdot \cos \alpha \cdot d\alpha + \int_{\alpha_1}^{\frac{\pi}{2}} \delta_s \cdot a_g^2 \cdot \tan \theta \cdot \cos \alpha \cdot d\alpha + \delta_b \cdot A_m$$

$$F_{nc}(a_g) = F_{nc(1)}(a_g) + F_{nc(01)}(a_g) + F_{nc(02)}(a_g)$$

$$= \left[\int_0^{\alpha_1} \delta_1(\alpha) \cdot d\alpha + \frac{\pi \cdot (\frac{\pi}{2} - \alpha_1)}{2 \cdot (1 - \sin \alpha_1)} \cdot \delta_b \cdot \tan \theta + (\frac{\pi}{2} - \alpha_1) \cdot \delta_s \right] \cdot a_g^2 \cdot \tan^2 \theta \quad (19)$$

3.4 Force model of cutting and ploughing grain

Material behavior in ploughing stage could be categorized as plastic flow, in which stress should reach at δ_s . Therefore, force model of ploughing grain could be calculated as Eqs. (20) and (21).

$$F_{ip}(a_g) = \int_0^{\frac{\pi}{2}} \delta_s \cdot a_g^2 \cdot \tan \theta \cdot \cos \alpha \cdot d\alpha \quad (20)$$

$$F_{np}(a_g) = \int_0^{\frac{\pi}{2}} \delta_s \cdot a_g^2 \cdot \tan^2 \theta \cdot d\alpha = \frac{\pi}{2} \cdot \delta_s \cdot a_g^2 \cdot \tan^2 \theta \quad (21)$$

3.5 Frictional force model

The frictional force is composed of rake face on ploughing grains $F_{pf}(a_g)$, rake face on cutting grains $F_{cf}(a_g)$, and the wear plane of the grain (f_n, f_t), as shown in Eqs. (22)–(30). The force magnitude is determined by stress and the lubricating state between the grains and the workpiece.

$$F_{pf}(a_g) = 2 \cdot \int_0^{\frac{\pi}{2}} \mu \cdot \delta_s \cdot ds = \int_0^{\frac{\pi}{2}} \mu \cdot \delta_s \cdot a_g^2 \cdot \frac{\tan \theta}{\cos \theta} \cdot d\alpha \quad (22)$$

$$F_{ipf}(a_g) = F_{pf}(a_g) \cdot \sin \theta = \int_0^{\frac{\pi}{2}} \mu \cdot \delta_s \cdot a_g^2 \cdot \tan^2 \theta \cdot d\alpha \quad (23)$$

$$F_{nfp}(a_g) = F_{pf}(a_g) \cdot \cos \theta = \int_0^{\frac{\pi}{2}} \mu \cdot \delta_s \cdot a_g^2 \cdot \tan \theta \cdot d\alpha \quad (24)$$

$$F_{cf}(a_g) = 2 \cdot \left(\int_0^{\frac{\pi}{2}} \mu \cdot \delta_0 \cdot ds + \int_0^{\alpha_1} \mu \cdot \delta_1 \cdot ds \right)$$

$$= \int_{\alpha_1}^{\frac{\pi}{2}} \mu \cdot \delta_0 \cdot a_g^2 \cdot \frac{\tan \theta}{\cos \theta} \cdot da + \int_0^{\alpha_1} \mu \cdot \delta_1 \cdot a_g^2 \cdot \frac{\tan \theta}{\cos \theta} \cdot da \quad (25)$$

$$F_{tcf}(a_g) = F_{cf}(a_g) \cdot \sin \theta = \int_{\alpha_1}^{\frac{\pi}{2}} \mu \cdot \delta_0 \cdot a_g^2 \cdot \frac{\tan \theta}{\cos \theta} \cdot da + \int_0^{\alpha_1} \mu \cdot \delta_1 \cdot a_g^2 \cdot \frac{\tan \theta}{\cos \theta} \cdot da \quad (26)$$

$$F_{ncf}(a_g) = F_{cf}(a_g) \cdot \cos \theta = \int_{\alpha_1}^{\frac{\pi}{2}} \mu \cdot \delta_0 \cdot a_g^2 \cdot \tan \theta \cdot da + \int_0^{\alpha_1} \mu \cdot \delta_1 \cdot a_g^2 \cdot \tan \theta \cdot da \quad (27)$$

$$f_n = N_d \cdot S_w \cdot \bar{p} = \frac{4 \cdot P_0 \cdot S_w \cdot N_d \cdot V_w}{V_s \cdot D} = \frac{4 \cdot K_1 \cdot N_d \cdot V_w}{V_s \cdot D} \quad (28)$$

$$f_t = \mu \cdot N_d \cdot S_w \cdot \bar{p} = \frac{4 \cdot \mu \cdot P_0 \cdot \delta \cdot N_d \cdot V_w}{V_s \cdot D} = \frac{4 \cdot \mu \cdot K_1 \cdot N_d \cdot V_w}{V_s \cdot D} \quad (29)$$

$$K_1 = P_0 \cdot S_w \quad (30)$$

where K_1 is the physical quantity related to the grain's wear state of the grinding wheel, which could be reversely solved through grinding experiment, and μ is the friction coefficient between the workpiece and the grains, which could be obtained by tribological tests [40].

4. Grinding force model and prediction

4.1 Procedure of modeling common grinding wheel

The matrix of the location distribution of the grains in the grinding zone is established as $G(z_g)$. The matrix of the protrusion height of the grains can be calculated as [40]:

$$G(z) = \frac{G(d)}{2} + G(z_g) = \begin{bmatrix} z_{11} & z_{12} & \cdots & z_{1N_y} \\ z_{21} & z_{22} & \cdots & z_{2N_y} \\ \vdots & \vdots & \ddots & \vdots \\ z_{N_x1} & z_{N_x1} & \cdots & z_{N_xN_y} \end{bmatrix} \quad (31)$$

4.2 Dynamic active grains in grinding zone

For two continuous cutting grains, maximum undeformed chip thickness $a_{g\max}$ ($a_g = 0.5a_{g\max}$ [42]) could be solved as [41, 42]:

$$a_{g\max} = 2 \cdot \lambda \cdot \frac{V_w}{V_s} \cdot \sqrt{\frac{a_p}{D}} \quad (32)$$

where λ is the space between the continuous cutting grains, D is the diameter of the grinding wheel, V_w is the feed speed, and V_s is the peripheral speed of the grinding wheel.

For common grinding wheel, λ value represented the space between the dynamic active grains. The equation of the n th grain is deduced as:

$$a_{g\max(n)} = 2 \cdot \lambda_{(n \sim n-1)} \cdot \frac{V_w}{V_s} \cdot \sqrt{\frac{a_p}{D}} + (a_{p(n)} - a_{p(n-1)}) \quad (33)$$

where $a_{g\max(n)}$ is the maximum undeformed chip thickness of the n th dynamic active grain, $\lambda_{(n \sim n-1)}$ is the space between the n th and the $(n - 1)$ th dynamic active grains, $a_{p(n)}$ is the protrusion height of the n th dynamic active grain, and $a_{p(n-1)}$ is the protrusion height of the $(n - 1)$ th dynamic active grain.

4.3 Grinding force model

Concrete calculation of grinding force can be described in **Figure 13**; the grinding force can be expressed in Eqs. (34) and (35).

$$F_t = \sum_1^{N_c} [F_{tc}(a_{gn}) + F_{tcf}(a_{gn})] + \sum_1^{N_p} [F_{tp}(a_{gm}) + F_{tpf}(a_{gm})] + f_t \quad (34)$$

$$F_n = \sum_1^{N_c} [F_{nc}(a_{gn}) - F_{ncf}(a_{gn})] + \sum_1^{N_p} [F_{np}(a_{gm}) - F_{npf}(a_{gm})] + f_n \quad (35)$$

where F_t/F_n are the tangential/normal grinding force, respectively, and f_t/f_n are the tangential/normal frictional force on the wear plane of grains, respectively. For the n th cutting grains ($1 \leq n \leq N_c$), a_{gn} is the cutting depth; $F_{tc}(a_{gn})/F_{nc}(a_{gn})$ are the tangential/normal cutting force, respectively; and $F_{tcf}(a_{gn})/F_{ncf}(a_{gn})$ are the tangential/normal frictional force on the rake face of the cutting grain, respectively. For the m th ploughing grains ($1 \leq n \leq N_c, N_c + N_p = N_d$), a_{gm} is the cutting depth; $F_{tp}(a_{gm})/F_{np}(a_{gm})$ are the tangential/normal, respectively; and $F_{tpf}(a_{gm})/F_{npf}(a_{gm})$ are the tangential/normal frictional force on the rake face of ploughing grain, respectively.

4.4 Experimental verification

MoS₂-palm oil nanofluid minimum quantity lubrication grinding experiment was carried out with K-P36 surface grinder. Prediction and experimental force values was shown in **Figure 14**.

The average percentage of the deviation in the normal force is 4.19%, while in the tangential force is 4.31%. For a certain grinding condition (dry grinding, $V_s = 20$ m/s, $V_w = 2$ m/min, $a_p = 15 \mu\text{m}$), the contribution of the tangential frictional force in the total tangential grinding force is approximately 89.17% and approximately 90.71% for normal force. However, it was decreased to 86.52% and 89.43% for tangential and normal direction, respectively.

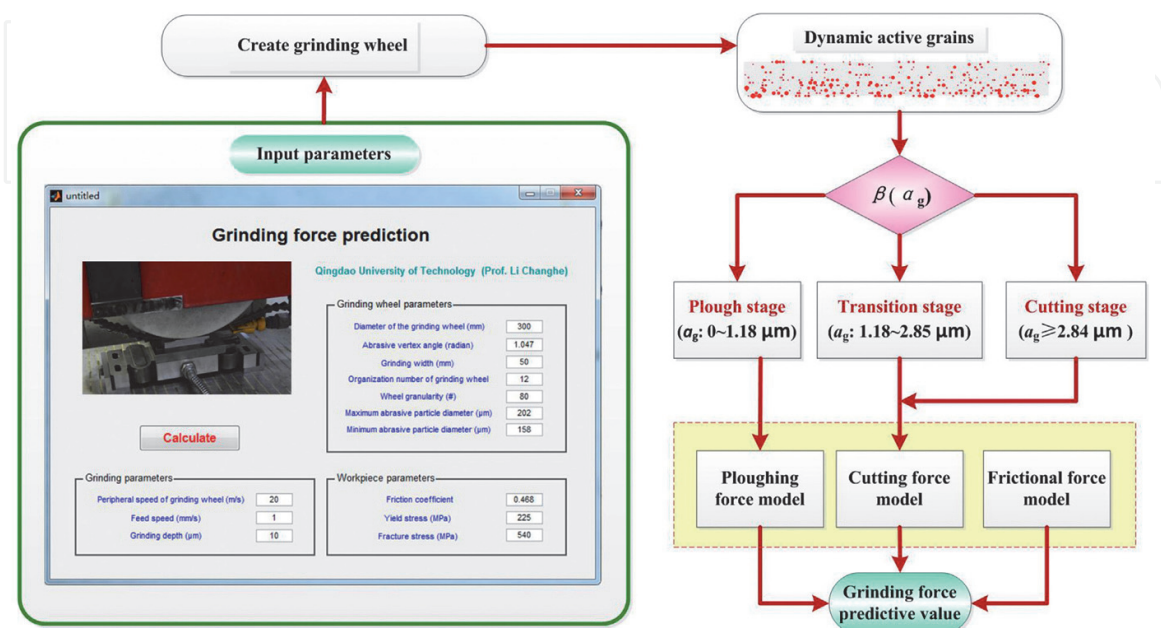


Figure 13.
 Process of the grinding force predictive program.

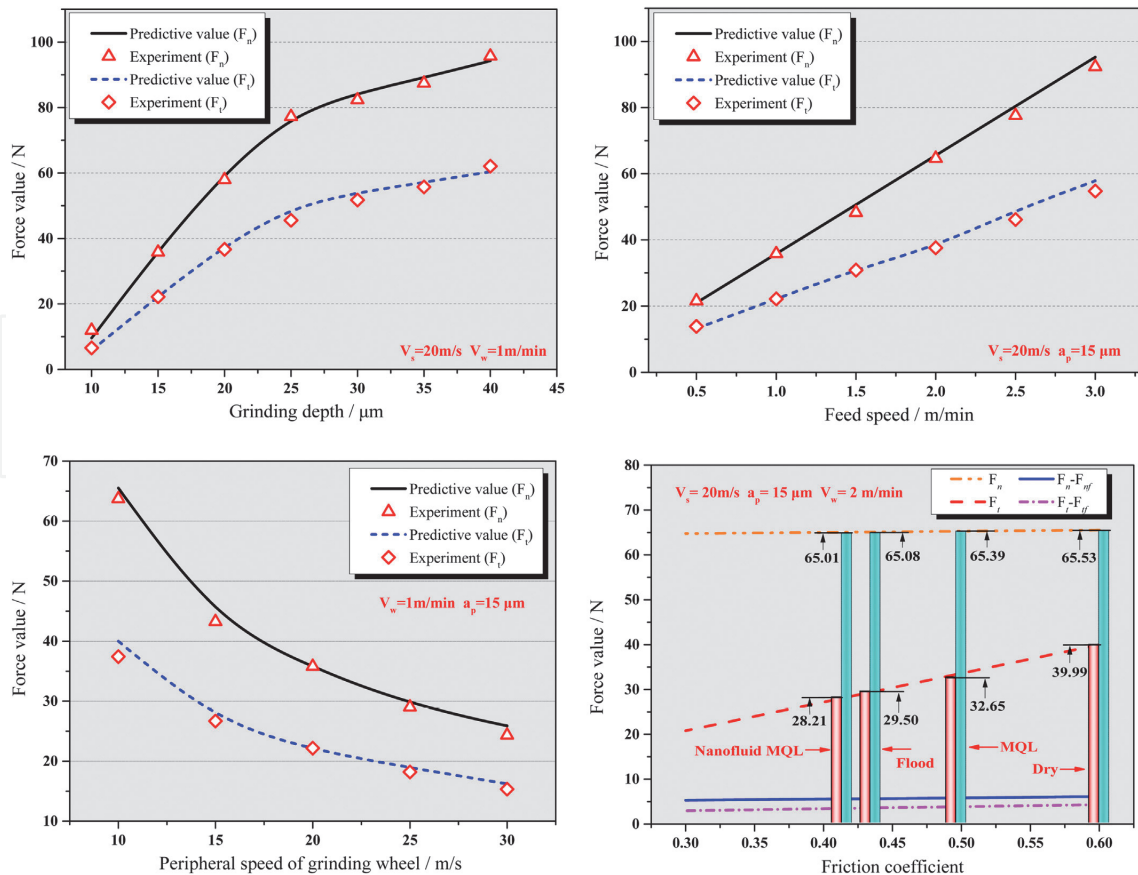


Figure 14.
Force prediction and experiment result.

5. Conclusions

To develop a model based on the stress state of a single grain, this study investigated the material removal mechanism and interference action in the grinding zone. The combined effect of the material removal and plastic stacking of a single grain has been considered.

Cutting experiment of single grain was carried out to obtain the critical cutting depth of the cutting and ploughing states. Results indicated that the variation trend of the grain-cutting efficiency (β) presents an S-shaped trend as the cutting depth (a_g) increases.

This study also developed and verified an improved grinding force predictive model. The average percentage of the deviation in the normal force is 4.19%, whereas that in the tangential force is 4.31%.

Acknowledgements

This research was financially supported by the following organizations: the National Natural Science Foundation of China (51975305 and 51905289), the Major Research Project of Shandong Province (2019GGX104040, 2019GSF108236, and 2018GGX103044), and the Shandong Provincial Natural Science Foundation of China (ZR2019PEE008), Major Science and technology innovation engineering projects of Shandong Province (2019JZZY020111), Applied basic research Youth Project of Qingdao science and technology plan (19-6-2-63-cg).

Conflict of interest

The authors declare no conflict of interest.

IntechOpen

Author details

Yanbin Zhang^{1,2}, Changhe Li^{1*}, Yongjun Zhao^{2*}, Xin Cui¹, Xiufang Bai³,
Mingzheng Liu¹, Yali Hou¹, Min Yang¹, Naiqing Zhang⁴, Heju Ji⁵, Xiaoming Wang¹
and Teng Gao¹

1 School of Mechanical Engineering, Qingdao University of Technology, Qingdao, China

2 MH Robot and Automation Co., Ltd., Weifang, China


3 School of Mechanical and Electrical Engineering, Qingdao Binhai University, Qingdao, China

4 Shanghai Jinzhao Energy Saving Technology Co. Ltd., Shanghai, China

5 Qingdao Dong Jia Textile Machinery Group Co., Ltd., Qingdao, China

*Address all correspondence to: sy_lichanghe@163.com; 18622115276@163.com

IntechOpen

© 2020 The Author(s). Licensee IntechOpen. Distributed under the terms of the Creative Commons Attribution - NonCommercial 4.0 License (<https://creativecommons.org/licenses/by-nc/4.0/>), which permits use, distribution and reproduction for non-commercial purposes, provided the original is properly cited. 

References

- [1] Zhang YB, Li CH, Jia DZ, et al. Experimental evaluation of the lubrication performance of MoS₂/CNT nanofluid for minimal quantity lubrication in Ni-based alloy grinding. *International Journal of Machine Tools & Manufacture*. 2015;**99**:19-33. DOI: 10.1016/j.ijmachtools.2015.09.003
- [2] Yang M, Li CH, Zhang YB, et al. Research on microscale skull grinding temperature field under different cooling conditions. *Applied Thermal Engineering*. 2017;**126**:525-537. DOI: 10.1016/j.applthermaleng.2017.07.183
- [3] Jia DZ, Li CH, Zhang YB, et al. Experimental evaluation of surface topographies of NMQL grinding ZrO₂ ceramics combining multiangle ultrasonic vibration. *The International Journal of Advanced Manufacturing Technology*. 2019;**100**(1-4):457-473. DOI: 10.1007/s00170-018-2718-y
- [4] Wu WT, Li CH, Yang M, et al. Specific Energy and G ratio of Grinding Cemented Carbide under Different Cooling and Lubrication Conditions. *The International Journal of Advanced Manufacturing Technology*. 2019;**105**(1-4):67-82. DOI: 10.1007/s00170-019-04156-5
- [5] Wang YG, Li CG, Zhang YB, et al. Comparative evaluation of the lubricating properties of vegetable-oil-based nanofluids between frictional test and grinding experiment. *Journal of Manufacturing Processes*. 2017;**26**:94-104. DOI: 10.1016/j.jmapro.2017.02.001
- [6] Li HN, Xie KG, Wu B, Zhu WQ. Generation of textured diamond abrasive tools by continuous-wave CO₂ laser: Laser parameter effects and optimisation. *Journal of Materials Processing Technology*. 2020;**275**:116279. DOI: 10.1016/j.jmatprotec.2019.116279
- [7] Li HN, Yang Y, Zhao YJ, et al. On the periodicity of fixed-abrasive planetary lapping based on a generic model. *Journal of Manufacturing Processes*. 2019;**44**:271-287. DOI: 10.1016/j.jmapro.2019.05.036
- [8] Gao T, Zhang XP, Li CH, et al. Surface morphology evaluation of multi-angle 2D ultrasonic vibration integrated with nanofluid minimum quantity lubrication grinding. *Journal of Manufacturing Processes*. 2020;**51**:44-61. DOI: 10.1016/j.jmapro.2020.01.024
- [9] Zhang YB, Li CH, Jia DZ, et al. Experimental evaluation of MoS₂ nanoparticles in jet MQL grinding with different types of vegetable oil as base oil. *Journal of Cleaner Production*. 2015;**87**:930-940. DOI: 10.1016/j.jclepro.2014.10.027
- [10] Yang M, Li CH, Zhang YB, et al. Predictive model for minimum chip thickness and size effect in single diamond grain grinding of zirconia ceramics under different lubricating conditions. *Ceramics International*. 2019;**45**(12):14908-14920. DOI: 10.1016/j.ceramint.2019.04.226
- [11] Yang M, Li CH, Zhang YB, et al. Maximum undeformed equivalent chip thickness for ductile-brittle transition of zirconia ceramics under different lubrication conditions. *International Journal of Machine Tools and Manufacture*. 2017;**122**:55-65. DOI: 10.1016/j.ijmachtools.2017.06.003
- [12] Werner G. Influence of work material on grinding forces. *CIRP Annals*. 1978;**27**:243-248
- [13] Malkin S, Hwang TW. Grinding mechanisms for ceramics. *CIRP Annals*. 1996;**45**(2):569-580. DOI: 10.1016/S0007-8506(07)60511-3
- [14] Li L, Fu J, Peklenik J. A study of grinding force mathematical model.

- CIRP Annals. 1980;**29**(1):245-249. DOI: 10.1016/S0007-8506(07)61330-4
- [15] Younis M, Sadek MM, El-Wardani T. A new approach to development of a grinding force model. *Journal of Engineering Industry*. 1987;**109**(4): 306-313
- [16] Tang J, Du J, Chen Y. Modeling and experimental study of grinding forces in surface grinding. *Journal of Materials Processing Technology*. 2009;**209**(6): 2847-2854. DOI: 10.1016/j.jmatprotec.2008.06.036
- [17] Hecker RL, Liang SY, Wu XJ, et al. Grinding force and power modeling based on chip thickness analysis. *The International Journal of Advanced Manufacturing Technology*. 2007;**33**(5-6):449-459. DOI: 10.1007/s00170-006-0473-y
- [18] Lang X, He Y, Tang J, et al. Grinding force model based on prominent height of abrasive submitted to Rayleigh distribution. *Journal of Central South University (Science and Technology)*. 2014;**45**(10):3386-3391
- [19] Zhang J, Ge P, Zhang L. Research on the grinding force based on the probability statistics. *China Mechanical Engineering*. 2007;**18**(20): 2399-2402
- [20] Chang CH, Wang J-JJ. A stochastic grinding force model considering random grit distribution. *International Journal of Machine Tools and Manufacture*. 2008;**48**(12-13): 1335-1344. DOI: 10.1016/j.ijmachtools.2008.05.012
- [21] Cheng J, Wu J, Gong YD, et al. Grinding forces in micro slot-grinding (MSG) of single crystal sapphire. *International Journal of Machine Tools and Manufacture*. 2017;**112**:7-20. DOI: 10.1016/j.ijmachtools.2016.10.004
- [22] Zhou M, Zheng W. A model for grinding forces prediction in ultrasonic vibration assisted grinding of SiCp/Al composites. *The International Journal of Advanced Manufacturing Technology*. 2016;**87**(9-12):3211-3224. DOI: 10.1007/s00170-016-8726-x
- [23] Jiang Z, Yin Y, Wang Q, et al. Predictive modelling of grinding force considering wheel deformation for toric optical mirrors. *Journal of Manufacturing Science and Engineering*. 2016;**138**(6):061008. DOI: 10.1115/1.4032084
- [24] Li HN, Yu TB, Wang ZX, et al. Detailed modeling of cutting forces in grinding process considering variable stages of grain-workpiece micro interactions. *International Journal of Mechanical Sciences*. 2017;**126**:319-339. DOI: 10.1016/j.ijmecsci.2016.11.016
- [25] Younis MA, Alawi H. Probabilistic analysis of the surface grinding process. *Transactions of the Canadian Society for Mechanical Engineering*. 1984;**8**(4): 208-213. DOI: 10.1139/tcsme-1984-0031
- [26] Zhang Y, Li C, Yang M, et al. Experimental evaluation of cooling performance by friction coefficient and specific friction energy in nanofluid minimum quantity lubrication grinding with different types of vegetable oil. *Journal of Cleaner Production*. 2016;**139**: 685-705. DOI: 10.1016/j.jclepro.2016.08.073
- [27] Cui X, Li C, Zhang Y, Jia D, Zhao Y, Li R, et al. Tribological properties under the grinding wheel and workpiece interface by using graphene nanofluid lubricant. *The International Journal of Advanced Manufacturing Technology*. 2019;**104**(9-12):3943-3958. DOI: 10.1007/s00170-019-04129-8
- [28] Zhang ZY, Wang B, Kang RK, et al. Changes in surface layer of silicon wafers from diamond scratching. *CIRP Annals*. 2015;**64**(1):349-352. DOI: 10.1016/j.cirp.2015.04.005

- [29] Cao JG, Wu YB, Li JY, et al. A grinding force model for ultrasonic assisted internal grinding (UAIG) of SiC ceramics. *The International Journal of Advanced Manufacturing Technology*. 2015;**81**(5-8):875-885. DOI: 10.1007/s00170-015-7282-0
- [30] Zhang Z, Guo D, Wang B, et al. A novel approach of high speed scratching on silicon wafers at nanoscale depths of cut. *Scientific Reports*. 2015;**5**:16395. DOI: 10.1038/srep16395
- [31] Zhang Z, Guo L, Cui J, et al. Nanoscale solely amorphous layer in silicon wafers induced by a newly developed diamond wheel. *Scientific Reports*. 2016;**6**:35269. DOI: 10.1038/srep35269
- [32] Zhang J, Song Y, Huo F, et al. Nanoscale material removal mechanism of soft-brittle HgCdTe single crystals under nanogrinding by ultrafine diamond grits. *Tribology Letters*. 2012;**46**(1):95-100. DOI: 10.1007/s11249-012-9924-9
- [33] Ding W, Dai J, Zhang LC, et al. An investigation on the chip formation and forces in the grinding of Inconel718 alloy using the single-grain method. *Issues in Mental Health Nursing*. 2014;**28**:1-2. DOI: 10.1016/j.ijmachtools.2017.06.002
- [34] Jin T, Stephenson DJ. Heat flux distributions and convective heat transfer in deep grinding. *International Journal of Machine Tools and Manufacture*. 2006;**46**(14):1862-1868. DOI: 10.1016/j.ijmachtools.2005.11.004
- [35] Zhang J, Wang Y, Wang Y. Experiment and constitutive model of rate-dependent behavior of titanium alloy TC11. *The Chinese Journal of Nonferrous Metals*. 2017;**27**(07): 1369-1375. DOI: 10.19476/j.ysxb.1004.0609.2017.07.07
- [36] Xun C, Rowe WB. Analysis and simulation of the grinding process. Part II: Mechanics of grinding. *International Journal of Machine Tools and Manufacture*. 1996;**36**(8):883-896. DOI: 10.1016/0890-6955(96)00117-4
- [37] Du HJ, Rui YN, Wang R, et al. MATLAB-based simulation method of surface's three-dimensional model in grinding process. *Modern Manufacturing Engineering*. 2009;(02): 48-51. DOI: CNKI:SUN:XXGY.0.2009-02-013
- [38] Öpöz TT, Chen X. Effect of different parameters on grinding efficiency and its monitoring by acoustic emission. *Production & Manufacturing Research*. 2016;**4**(1): 190-208. DOI: 10.1080/21693277.2016.1255159
- [39] Lindsay RP, Hahn RS. *Principle of Grinding, Part I, II*. Machinery. 1971
- [40] Zhang Y, Li C, Ji H, et al. Analysis of grinding mechanics and improved predictive force model based on material-removal and plastic-stacking mechanisms. *International Journal of Machine Tools and Manufacture*. 2017;**122**:81-97. DOI: 10.1016/j.ijmachtools.2017.06.002
- [41] Agarwal S, Venkateswara Rao P. Predictive modeling of force and power based on a new analytical undeformed chip thickness model in ceramic grinding. *International Journal of Machine Tools and Manufacture*. 2013;**65**:68-78. DOI: 10.1016/j.ijmachtools.2012.10.006
- [42] Cai R, Qi HS, Cai GQ. Active cutting edges in vitrified CBN grinding wheels. *Key Engineering Materials*. 2006;**304**: 1-7. DOI: 10.4028/www.scientific.net/KEM.304-305.1